Biogeosciences
Discussions

Dinocyst assemblage constraints on oceanographic and atmospheric processes in the Eastern Equatorial Atlantic over the last 44 ka

Hardy William [a] *, **Penaud Aurélie** [a] *, **Marret Fabienne** [b], **Bayon Germain** [c], **Marsset Tania** [c], **Droz Laurence** [a]

(a) UMR 6538 Domaines Océaniques, IUEM-UBO, F-29280 Plouzané, France.

(b) School of Environmental Sciences, University of Liverpool, Liverpool, L69 7ZT, UK

(c) IFREMER, UR Géosciences Marines, BP 70-29280 Plouzané, France

*Corresponding author. Tel.: +33-298-498-741; fax: +33-298-498-760

E-mail address: william.hardy@univ-brest.fr

17 **ABSTRACT**

18 A new 44 ky-long record of dinoflagellate (phytoplanktonic organisms) cysts (dinocysts) is

19 presented from a marine sediment core collected on the Congolese margin with the aim to

20 reconstruct past hydrological changes of the Equatorial Eastern Atlantic Ocean since Marine

21 Isotopic Stage 3. Our high-resolution dinocyst record indicates that significant temperature

22 and moisture variations occurred across the glacial period, the last deglaciation and the

23 Holocene. The use of specific dinocyst taxa, indicative of fluvial, upwelling and Benguela

24 Current past environments for instance, provides insights into the main forcing mechanisms

25 controlling paleohydrological changes at orbital timescales. In particular, we are able, for the

26 last 44 ky to correlate fluvial-sensitive taxa to monsoonal mechanisms related to precession

27 minima/obliquity maxima combinations. While upwelling mechanisms appear as the main

28 driver for dinoflagellate productivity during MIS 2, dissolved nutrient-enriched Congo River

29 inputs to the ocean also played a significant role in promoting dinoflagellate productivity

30 between approximately 15.5 and 5 ka BP. Finally, this high resolution dinocyst study permits

31 to precisely investigate the sub-orbital timing of the last glacial-interglacial termination

32 including an atypical warm and wet oceanic LGM signature, northern high latitude abrupt

33 climate change impacts in the Equatorial Eastern Atlantic, as well as a two-steps mitigation of

34 moisture conditions during the Holocene at around 7-6 and 4-3.5 ka BP.

35 .

36 *KEYWORDS: Dinoflagellate cysts; Congolese margin; Deglaciation; Holocene;*

37 *Paleoproductivity; Monsoon dynamic*

38

39

Biogeosciences

Discussions

Open Access

1. INTRODUCTION

Reconstructions of Late Quaternary and Holocene paleoceanographic changes at the Western African margin and associated Benguela upwelling system have identified orbital and sub-orbital controls on sea-surface and continental environmental conditions (Holzwarth et al., 2007). More specifically, several palynological studies carried out in the Equatorial Eastern Atlantic Ocean, combining analysis of pollen grains and cysts of dinoflagellates (dinocysts), have provided a wealth of information on land-sea interactions in the intertropical region, through investigation of sea-surface and terrestrial vegetation changes over the last climatic cycles (Shi et al., 1998; Marret and Zonneveld, 2003; Dupont and Behling, 2006; Marret et al., 2008; Kim et al., 2010; Bouimetarhan et al., 2012; Marret et al., 2013). However, these above-mentioned studies mainly focused on the comparison between periods of extreme climatic conditions, such as the Last Glacial Maximum (Mix et al., 2001) and the Holocene Climatic Optimum, showing that higher primary productivity conditions occurred during glacial periods in response to an increase of upwelling activity while enhanced freshwater discharges from the continent occurred during interglacials. In comparison, the Last Deglaciation period, which consisted in a shift from upwelled cold waters (associated with dry conditions on land - glacial) to monsoonal regimes (associated with warm waters offshore - interglacial), has been less studied and its timing in this area remains poorly defined, mainly due to a lack of high-resolution investigations.

In this study, we have investigated a marine sediment core (KZAI-01) recovered during the ZaiAngo I cruise (Savoye et al., 2000) at the West-African continental slope, upstream the Congo deep-sea fan. This core is characterized by a high average sedimentation rate (about 25 cm/ka, maximum of 50 cm/ka) that enables to provide high-resolution paleoenvironmental records for the last 44 ka (Bayon et al., 2012). We have combined new dinocyst analysis with a set of already published geochemical data for sediment provenance and weathering proxies

Biogeosciences

Discussions

Open Access

EGU

65 (Bayon et al., 2012). The comparison between terrestrial and marine proxy data can then be

66 used to discuss about the links between environmental changes that have occurred in the

67 Congo catchment area and past sea-surface oceanographic through dinoflagellate productivity

68 variations.

69 Several objectives have motivated this study:

70   1) To document the potential of dinocysts for reconstructing sea-surface environments in

71   the Eastern Atlantic Ocean and discussing about the links between continental and

72   hydrological changes over the last 44 ka,

73   2) To discuss orbital forcing impacts in our recorded dinocyst observations and the

74   potential influence of the monsoonal activity on sea-surface past conditions,

75   3) To precisely characterize, in the Equatorial Atlantic Ocean, the timing of the Last

76   Deglaciation at a millennial time-scale resolution.

77

78 **2. ENVIRONMENTAL CONTEXT ON THE CONGOLESE MARGIN**

79 The Congo River drains the second catchment area of the world with a total surface of

80 3,600,000 km² and a mean flow of 41,000 m^3/s. This river feeds the Congo deep-sea fan

81 (Babonneau et al., 2002; Droz et al., 2003; Savoye et al., 2009; Picot et al., 2016), one of the

82 largest deep-sea fans in the world, *via* a submarine Pliocene canyon (Anka et al., 2009) still

83 active at present (Heezen and Hollister, 1964; Khripounoff et al., 2003)

84 *2.1. Present-day atmospheric context*

85 Climatic patterns in the Congo Basin are controlled by the seasonal latitudinal migration of

86 the Tropical Rainbelt (TR, Fig. 1), which is associated offshore with high sea-surface

87 temperatures (SST) and low salinities (Zarriess and Mackensen, 2010; Arbuszewski et al.,

88 2013). This low pressure belt is characterized by moist air ascension and large tropical

89 rainstorms, generated by the association of the Tropical and African Easterly Jets in the

Biogeosciences
Discussions

Open Access

EGU

90   Northern Hemisphere (Nicholson, 2009). The TR and the Inter Tropical Convergence Zone

91   (ITCZ) constitute the complex convective system of African monsoon. which shift seasonally

92   from a northward position during boreal summer to a southward position during boreal winter

93   (Hsu and Wallace, 1976). While the central part of the Congo Basin is characterized by an

94   equatorial regime, its northern and southern parts alternate between wet and dry seasons

95   (Prance, 1984; Leroux, 2001). This results in a latitudinal distribution of the vegetation from

96   rainforests to savannahs across the whole Basin (Prance, 1984). Easterly winds from the

97   Indian Ocean also brings moisture to the Congo Basin, in particular during the austral

98   summer, due to the presence of the Congo Air Boundary convergence zone (CAB, Tierney et

99   al., 2011), also evidencing the influence of the eastern African monsoon system in central

100   Africa.

101

102   *2.2. Present-day oceanographic context*

103   Surface water masses from the Congolese margin are largely influenced by the Angola

104   Current (AC; Figure 1), a clockwise subequatorial gyre located above the north-eastern part of

105   the Subtropical Gyre (Lass and Mohrholz, 2008). The warm waters of the AC meet the cool

106   waters of the couple Benguela Current and Coastal Benguela Current (BC and cBC; Figure 1)

107   at around 16°S at the Angola-Benguela Front (Lass and Mohrholz, 2008). This cool surface

108   current causes weak evaporation and aridity conditions on the adjacent continent (Gordon et

109   al., 1995), as well as water mass stratification on the continental shelf, itself depleted in

110   oxygen (Gordon et al., 1995).

111   The South Atlantic Anticyclone, driving the Subtropical Gyre, generates SE trade winds on

112   the SW African margin, and consequently upwelling cells throughout the BC (Gordon et al.,

113   1995; Lass and Mohrholz, 2008). These upwelled waters bring deep nutrient-rich waters that

114   promote high primary productivity in surface waters. The Benguela upwelling system is

115   limited northward around the ABF location (Jansen et al., 1996; Lass and Mohrholz, 2008).

116   Congo River freshwater discharges also exert an influence on the regional oceanographic

117   setting, in particular because of the relative weakness of the Coriolis force near the Equator

118   that allows river plumes to extend far from the coast (da Cunha and Buitenhuis, 2013). This

119   mechanism also contributes to promote fluvial upwelling and thus to additional nutrients

120   exported to surface waters. Today, rainforests prevent soils from active erosion and therefore

121   prevent the delivery of substantial fluvial nutrient supplies to the Gulf of Guinea.

122

123   **3. MATERIAL AND METHODS**

124   *3.1. Stratigraphy of core KZAI-01*

125   Core KZAI-01 (5°42.19'S; 11°14.01'E; 816 m water depth; 10.05 m length; Figure 1) was

126   recovered during the 1998 ZaiAngo 1 cruise aboard the *Atalante* (Savoye, 1998).

127   First published age model of core KZAI-01 (Bayon et al., 2012) was derived from (Table 1)

128   seven AMS ^{14}C dates on carbonates (bulk planktonic foraminifera or mixed marine

129   carbonates), and two age constraints obtained by tuning core KZAI-01 to core GeoB6518-1

130   (well-dated sedimentary record from the nearby area; Figure 1) (Bayon et al., 2012).

131   In this study, three new AMS ^{14}C dates on carbonates have been added between 370 and 620

132   cm so as to obtain a more robust stratigraphy for the Last Glacial period (Table 1; Figure 2).

133   We have also added three new age constraints obtained by tuning core KZAI-01 to well dated

134   nearby core GeoB6518-1 (AMS ^{14}C dates on monospecific foraminifera; Schefuss et al.,

135   2005; Figure 2). This enables us to strengthen the chrono-stratigraphy of the study core for the

136   Early Holocene as well as for the base of KZAI-01 core, not constrained by AMS ^{14}C dates

137   below 851 cm.

138   All radiocarbon dates were calibrated to calendar ages with the 7.0 Calib program associated

139   with a 400 years correction for the marine age reservoir (Minze Stuiver, 1992; Reimer, 2013),

140 and the final age model was built through linear regression between all stratigraphic pointers

141 (cf. Table 1; Figure 2). Mean calculated sedimentation rates are around 25 cm/ky.

142

143 *3.2. Palynological analysis*

144 *3.2.1. Laboratory procedure for dinocyst extraction*

145 In this study, 203 samples were analysed for the period covering the last 44 ka with a 5 cm

146 sampling interval (mean resolution analysis of about 200 years throughout the core, ranging

147 between 20 and 800 years, according to the established age model). The preparation technique

148 for palynological analysis followed the procedure described in Marret et al. (2008). Calibrated

149 tablets of known concentrations of *Lycopodium* spores were added in each sample before

150 chemical treatments in order to estimate palynomorph concentrations (number of

151 dinocysts/cm^3 of dry sediments), and chemical and physical treatments included cold HCl

152 (10%), cold HF (40%), and sieving through a single use 10 μm nylon mesh screen. The final

153 residue was mounted between slide and coverslip with glycerine jelly coloured with fuschin.

154 When the recommended number of 300 dinocysts could not be reached, a minimum of 100

155 specimens was counted on each sample (F Fatela, 2002), using a Leica DM 2500 microscope

156 at ×630 magnification. Fifteen samples, containing less than 100 specimens, were excluded

157 from the dinocyst results. Dinocyst concentrations were based on the marker grain method (de

158 Vernal et al., 1999) and dinocyst assemblages were described by the percentages of each

159 species calculated on the basis of the total dinocyst sum including unidentified taxa and

160 excluding pre-Quaternary specimens. In addition to dinocyst counts, freshwater microalgae

161 *Pediastrum* and *Concentricystes* were also identified and counted so as to discuss river

162 discharge intensifications in parallel with our dinocyst data.

163

164

165   *3.2.2. Dinocysts as potential witnesses for past primary productivity changes*

166   Paleoproductivity regimes in the Equatorial Ocean can be inferred from our fossil

167   assemblages thanks to the transfer function based on the Modern Analogue Technique (MAT;

168   Guiot and de Vernal, 2007) developed for the Tropical Atlantic Ocean (n=208 modern

169   analogues; Marret et al., 2008). Mean annual Primary Productivity (PROD_Modis, Radi et al.,

170   2008 and PROA, Antoine et al., 1996) can then be quantified with a prediction error of 65,07

171   g/m². However, results issued from these quantifications include a number of limitations and

172   criticisms that will be discussed later in a paper devoted to primary productivity regimes in

173   the study area with an extended space vision and a data-model inter-comparison approach. In

174   this paper, we only focus on the dinoflagellate phytoplanktonic compartment through past

175   dinocyst specific observations. Indeed, among dinocyst assemblages, it is possible

176   distinguishing between cysts formed by dinoflagellates with a strict nutritional strategy based

177   on heterotrophy that we will refer as "heterotrophic cysts", and other cysts formed by

178   dinoflagellates for which the nutritional strategy can be complex involving either autotrophy,

179   heterotrophy or mixotrophy and that we will refer as "non heterotrophic cysts". It is well

180   known that relative abundances of total heterotrophic cysts can be used as a signal for

181   dinoflagellate primary productivity, and indirectly for marine productivity, considering that

182   heterotrophic dinoflagellates mainly feed on marine micro-organisms including other

183   dinoflagellates (whatever their nutritional strategies), diatoms and other micro-algae (e.g

184   Zonneveld et al., 2013).

185

186   **4. DINOCYST RESULTS ON CORE KZAI-01**

187   ***4.1 Dinocyst concentrations***

188   A total of 53 different dinocyst taxa (Annexe 1) have been identified in the studied samples,

189   with an average of 15 different taxa for each sample (Figure 3). Total dinocyst absolute

190   concentrations in sediments are generally very low, from 100 cysts/cm^3 to 12,000 cysts/cm^3

191   (Figure 3). These low total concentrations in the study area are mainly attributed here to a

192   strong dilution of the organic matter by terrigenous inputs (cf. Figure 3 with the obvious

193   negative correlation between maximal values of terrestrial inputs (Ti/Ca and minimal values

194   of dinocyst concentrations), but also to a probable competition with diatom productivity

195   (Marret et al., 2008).

196   Higher total cyst concentrations are recorded between 850 and 450 cm (37.5 - 15.5 ka BP;

197   mean value of 3,000 cysts/cm^3), as well as between 90 and 30 cm (4 - 2.4 ka BP; mean value

198   of 6,000 cysts/cm^3), for which two maxima are observed with 10,900 and 11,200 cysts/cm^3,

199   respectively (Figure 3). Increases in total dinocyst concentrations can be mainly attributed to

200   increasing occurrences of *Operculodinium centrocarpum* or *Lingulodinium machaerophorum*

201   (Figure 3). Heterotrophic cyst concentrations (mainly led by *Brigantedinium* spp. and

202   *Echinidinium* species; Figure 3) as well as other cyst concentrations reach their maximal

203   values during the same main interval, i.e between 850 and 450 cm, but are three times lower

204   for heterotrophics (Figure 3). Also, higher total heterotrophic relative abundances, mainly

205   driven by *Brigantedinium* spp. percentages all along the record (Figure 3), as well as those of

206   *Echinidinium* spp. between 450 and 90 cm (15.5 - 4 ka BP; Figures 3 and 5), are strongly

207   correlated with lower total dinocyst concentrations, especially between 15 and 4 ka BP

208   (Figures 3 and 4). This could be consistent with the fact that diatoms, but also dinoflagellates,

209   consist in the main food for strict heterotrophic dinoflagellates (Marret and Zonneveld, 2003),

210   therefore echoing the previous idea of a competition between dinoflagellate and diatom

211   phytoplanktonic productivity in the study area (Marret and Zonneveld, 2003).

212   Even if heterotrophic dinocyst concentrations can firstly be attributed to

213   dilution/concentration processes in sediments, the transition between generally higher cyst

214   concentrations and lower ones observed at 450 cm (15.5 ka cal. BP) is synchronous with a

215   marked shift in biogenic silica (BiSiO$_2$) and total organic carbon (TOC) observed in a nearby

216   core (Schneider et al., 1997). This could lead us to suggest different marine productivity

217   patterns before and after 15.5 ka BP. Based at least on the fact that these data indicate

218   generally similar trends, an atypical pattern is however obvious at 90 cm. While heterotrophic

219   concentrations remain low, and despite a relative stable trend characterized by still high

220   terrigenous inputs (Bayon et al., 2012; Figure 3) and low BiSiO$_2$ and TOC values (Schneider

221   et al., 1997), total dinocyst concentrations reach their maximum. To understand this atypical

222   total dinocyst concentration signal, indexes of specific diversity and dominance have been

223   calculated so as to help us discussing periods possibly characterized by cyst advection

224   (positive correlation between dominance and diversity) and in situ dinoflagellate productivity

225   (negative correlation between dominance and diversity). Here, signals remain roughly anti-

226   correlated all over the core, except from 90 cm (Figure 3), perhaps involving massive

227   advection of *O. centrocarpum* at that time (Figure 3).

228

229   *4.2 Dinocyst assemblages*

230   Based on variations in cyst concentrations and in relative abundances of major species, five

231   palynozones (A, B, C, D, E; Figure 3) have been established, then subdivided into several

232   sub-palynozones (1, 2, 3; Figures 4 and 5) thanks to the rest of the assemblage (minor species

233   always observed with at least >2%; Figures 4 and 5).

234   Temporal successions between dinocyst species can be observed all along the core. This is

235   especially obvious regarding a dinocyst group mainly controlled by sea-surface salinity

236   (Marret and Zonneveld, 2003), including *Spiniferites ramosus*, *Nematosphaeropsis*

237   *labyrinthus*, *L. machaerophorum*, *O. centrocarpum* and *Operculodinium israelianum* (Figures

238   3, 4), as well as *Echinidinium* spp. (Figure 5). The first important succession occurred at 37.5

239   ka BP (limit between palynozones E and D), with a significant drop of the maximal

240   abundances of the couple *S. ramosus - N. labyrinthus*, then followed by maximal abundances

241   of *L. machaerophorum* (Figure 4). At 32 ka BP (limit between palynozones D and C), a

242   second major transition is related to a strong decline of *L. machaerophorum* synchronously

243   with maximal abundances of *O. centrocarpum* percentages, and then accompanied by *O.*

244   *israelianum* across whole palynozone C (Figure 4). A third succession (limit between

245   palynozone C and B) is then operated between *O. centrocarpum* and *Echinidinium* spp.

246   (Figures 4 and 5) at 15.5 ka cal. BP, while the last major transition (limit B-A) evidences the

247   important decline of *Brigantedinium* spp. and strong re-increase of *O. centrocarpum* from 6

248   ka BP onwards, together with the significant occurrence of *Spiniferites pachydermus* near the

249   start of palynozone A (a2, Figure 4).

250   Among non-heterotrophics, a group of thermophile species can be described with

251   *Impagidinium aculeatum, Impagidinium patulum, Spiniferites bentorii, Tuberculodinium*

252   *vancampoae, Spiniferites membranaceus* and *S. pachydermus*. This group also shows obvious

253   temporal successions across the different palynozones (cf. Figure 4). This is especially true

254   for *S. pachydermus* at the start of palynozone A (Figure 4). Concerning *Operculodinium*

255   *aguinawense* (Figure 4), the southernmost occurrences ever recorded of this species is here

256   observed with marine core KZAI-01. This species only occurs today off the coasts of

257   Cameroon and eastern Nigeria, in a small area encompassing GeoB4905 core (Marret and

258   Kim, 2009). Over the last 15.5 ka, variations of *O. aguinawense* percentages are relatively

259   well correlated with *Spiniferites mirabilis* ones, especially across the Last Deglaciation.

260   Today, both species are restricted to the same area along the north equatorial African coast

261   (Zonneveld et al., 2013).

262   Among heterotrophics, coastal taxa such as *P. schwartzii, Selenopemphix nephroides*, and

263   especially *Xandarodinium xanthum* as well as *Quinquecuspis concreta* (Figure 5), show

264   extremely close occurrences all along the core. This is especially obvious between 37 and 7

265 ka BP (Figure 5), and maximal abundances of these species are recorded around 36-32 ka, 25-

266 20 ka and 15.5-7 ka BP (Figure 5). Also, another important feature is the disappearance of *P.*

267 *schwartzii* around 35 ka BP, synchronously with *S. nephroides* significant increase at that time

268 (Figure 5; limit between sub-palynozones d2 and d1).

269

270 **5. DISCUSSION**

271 *5.1. Orbital control on past dinoflagellate productivity regimes*

272 *5.1.1. Dinoflagellate productivity on the Congolese margin: Congo River versus upwelling*

273 *dynamics*

274 Over the last glacial cycle, it is commonly admitted that higher primary productivity

275 conditions in the intertropical band occurred during periods of global cooling such as the

276 LGM or Greenland Stadials (GS, including Heinrich Stadials or HS), in response to

277 intensified upwelling cells. Inversely, during warmer and wetter periods such as Greenland

278 Interstadials (GI) or the Holocene characterized by higher riverine inputs (Dupont et al., 1998;

279 Shi et al., 1998; Dupont and Behling, 2006; Kim et al., 2010; Zonneveld et al., 2013), primary

280 productivity is low.

281 Within our dinocyst record, higher dinoflagellate productivity seems to be recorded during the

282 last glacial until 15.5 ka BP (high cyst concentrations and), consistently with high values of

283 Biogenic Silica (BiSiO$_2$) and Total Organic Carbon (TOC) observed in a neighbour core

284 (GeoB 1008; (Schneider et al., 1997). Furthermore, *Trinovantedinium applanatum*, a typical

285 well-known coastal upwelling species (Marret and Zonneveld, 2003), mainly occurred

286 between around 28 and 19 ka BP (palynozones c3 to c2; Figures 5 and 6), consistently with

287 the idea of stronger upwelling cells across glacial maxima, and more specifically here during

288 MIS 2, in a dry context characterized by weak terrigenous supplies to the Congo margin, and

289 cold sea-surface conditions as evidenced through *O. centrocarpum* higher percentages.

290   At the onset of the Last Deglaciation, around 15.5 ka BP, a quasi-disappearance of the *T.*

291   *applanatum* signal is observed (Figures 5 and 6). However, heterotrophic percentages remain

292   high and are even characterized, between 15.5 and 7 ka BP (sub-palynozones b2 and b3), by

293   the highest values ever recorded (Figures 5 and 6). This brings us to consider, at that time,

294   another major source of nutrients to the ocean than upwelling cells. The relatively good

295   consistency between major element terrestrial signals (cf. XRF ratios in KZAI-01 core, Figure

296   6), heterotrophic (*Brigantedinium* spp.) as well as fluvial-sensitive cyst (*Echinidinium* spp.,

297   river-plume taxa) percentages, suggests that nutrient-rich freshwater discharges from the

298   Congo River probably acted as a major driving factor for promoting dinoflagellate

299   productivity in the study area, especially across the Last Deglaciation, but also during MIS 3

300   (Figures 5 and 6). Furthermore, between 15.5 and 7 ka BP, continental shelf reworking,

301   induced by the post-glacial sea-level rise, may have also represented an additional source of

302   nutrients to the ocean (Marret et al., 2008), then also contributing to slightly enhanced

303   dinoflagellate productivity at that time (Figures 5 and 6).

304

305   *5.1.2 Precession versus Obliquity accounting for different fluvial regimes*

306   The influence of orbital forcing in low latitude atmospheric processes is still a matter of

307   debate. The tropical response to obliquity forcing appears to be the remote influence of high-

308   latitude glacial ice-sheet oscillations (deMenocal et al., 1993), in parallel with significant

309   changes in cross-equatorial insolation gradient (Bosmans et al., 2015). Precession forcing is

310   more important in low latitude moisture changes, i.e warmer and wetter conditions in the

311   hemisphere where summer solstice occurred at the Earth perihelion (Merlis et al., 2012).

312   Furthermore, it was evidenced that the combination precession/obliquity has also a great

313   influence in the monsoon oscillations with a significant prevalence of the precession forcing

314   (Tuenter et al., 2003). More precisely, minima of precession would correspond to an

Biogeosciences
Discussions

315   intensification of the monsoonal activity, and obliquity would tend to mitigate (minima of

316   obliquity) or enhance (maxima of obliquity) the initial precession forcing (Tuenter et al.,

317   2003). The orbital variations have therefore changed significantly the latitudinal widespread

318   of precipitations in consequence of oceanic heat gradient variations (Stager et al., 2011;

319   McGee et al., 2014).

320   In our dinocyst record, significant occurrences of fluvial-sensitive cysts (especially *L.*

321   *machaerophorum* and *Echinidinium* species) appear to correspond to minima of precession,

322   thus suggesting wetter conditions in the study area (Figure 6). This is especially observed

323   during the last Deglaciation-early Holocene between 16 and 6 ka BP (with the prevalence of

324   *Echinidinium* spp.), as well as during the MIS 3 interval between 39 and 32 ka BP (with the

325   prevalence of *L. machaerophorum*). Superimposed on this general scheme, a combination

326   "minimum of precession-maximum of obliquity" would explain the optimal orbital

327   combination for high moisture conditions according to Tuenter et al. (2003). This

328   configuration indeed occurred between 16 and 6 ka BP in our dinocyst results and

329   corresponds to the maximal recorded values of fluvial-sensitive cysts (*Echinidinium* spp.) in

330   combination with the highest values of heterotrophic cyst percentages (mainly including

331   *Brigantedinium* spp.; Figure 6).

332   The minimum of precession recorded during MIS 3 (Figure 6) is characterized by a

333   decreasing trend of Earth's obliquity, and is also consistently characterized by a weaker Ti/Ca

334   ratio and associated lower surface productivities between 39 and 32 ka BP (Figure 6). Despite

335   the austral location of KZAI-01, dinocyst assemblages indicate wetter conditions during

336   precession minima (Figure 6), i.e when Earth perihelion occurred during northern summer

337   solstice, with consequently associated drier conditions in the Southern Hemisphere (Merlis et

338   al., 2012). Conversely, maxima of precession, supposed to be favourable for wetter conditions

339   in the Southern Hemisphere, correspond to periods with lower terrigenous inputs, and

Biogeosciences

Open Access

Discussions

EGU

340   especially between 44 and 39 ka BP (subpalynnozone e2) and between 25 and 16 ka BP

341   (subpalynozones c2 and c1; Figure 6).

342

343   *5.1.3. The atypical signature of the MIS 2*

344   In the tropics, during MIS2, the latitudinal contraction of the TR resulted in colder conditions

345   on the continent (Powers et al., 2005; Tierney et al., 2011; Loomis et al., 2012) with the

346   establishment of open landscape (Anhuf et al., 2006), and cold surface waters (deMenocal et

347   al., 2000; Syee Weldeab, 2005; Shakun and Carlson, 2010). This general and commonly

348   admitted pattern is in agreement with the low terrigenous signal recorded on core KZAI-01

349   (Figure 6) that suggests reduced weathering conditions combined with lower terrestrial

350   erosion at that time. Paleo precipitation reconstructions (Bonnefille and Chalié, 2000) also

351   suggest generally low mean values of precipitations in the Congo Basin, however

352   characterized by a complex pattern oscillating between slightly wetter and drier conditions. In

353   our dinocyst record, slight occurrences of *T. applanatum*, *Selenopemphix quanta* (Figure 5)

354   and cysts of *Pentarpharsodinium dalei* (Annexe 1) are consistent with the tropical

355   climateuring glacial period, mainly influenced by upwelling mechanisms under dry climate.

356   However, between 25 and 17 ka BP (sub-palynozones c2 and c3; Figure 6), low abundances

357   of *Echinidinium* species as well as high percentages of *L. machaerophorum* (up to 50 %)

358   would suggest strengthened river discharges and thus wetter conditions consistently with the

359   general pattern of Austral moisture during maximal values of the precession index. The

360   lowered sea level influence on dinocyst assemblages, at that period, cannot be however totally

361   excluded regarding the neritic ecology of *L. machaerophorum*. However, another atypical

362   dinocyst signature of MIS2 relies on the occurrence of thermophile species (*S. mirabilis*, *S.*

363   *membranaceus*, *S. bentorii* and *T. vancampoae*; Figures 4 and 5) which mainly occurred

364   between 21 and 17 ka BP, after a gradual increase noted from the beginning of the LGM

365   (Figures 4 and 5). The southward shift of the TR and the equatorial warm waters until 2°S

366   (Arbuszewsky et al., 2013) may have brought heat and moisture within the study area while

367   other parts of the Equatorial Atlantic remained colder and drier (Stager et al., 2011). This

368   pattern can possibly be explained by the cross-equatorial location of the Congo Basin, also

369   benefiting from southern hemisphere wetter configurations. Northern Congo Basin

370   corresponds to a tierce of the whole surface but northern tributary rivers contribute to an half

371   of the total discharge (Bultot, 1971; Lempicka, 1971), it is however important to underline the

372   greater influence of northern rivers in comparison with austral ones within the Congo Basin;

373   terrigenous inputs to the ocean will then be more important when the northern basin will be

374   fed by strengthened precipitations in a boreal context of precession minima.

375

376   *5.1.4 Eastern and Western African monsoons: complex interferences in the Congo Basin*

377   The large scale of the Congo Basin raises the question of the complex interferences between

378   Western and Eastern African monsoon systems, i.e. the atmosphere above the catchment area

379   is divived by the Congo Air Boundary (CAB) convergence zone (Tierney et al., 2011),

380   displaying the border between the western and eastern African monsoon. Past oscillations of

381   these different monsoon clusters have been simulated (Caley et al., 2011; Figure 6) through

382   paleo river discharges of the Niger (Western African monsoon) and of the Nile (Eastern

383   African monsoon). As mentioned above, dinocyst river-plume assemblages of core KZAI-01

384   develop strongly in response to boreal summer river discharges linked with precession

385   minima (Figure 6), suggesting that the Western African monsoon can be considered as the

386   main forcing for northern summer rainfalls in the Congo Basin. This common pattern is

387   particularly well highlighted during the Last Deglaciation when river-plume taxa abundances

388   increase in parallel with terrigenous signals shortly after the increase of the Western African

389   monsoon around 16 ka BP (Figure 6). Furthermore, the maximum of the West African

390   monsoon activity, that occurred between 8 and 6 ka BP (Figure 6), also corresponds with the

391   highest occurrences of *O. aguinawense*, evidencing a great relationship between the western

392   African monsoonal forcing and the establishment of near equatorial conditions during this

393   period (Marret and Kim, 2009).

394   However, the suitable relationship described above between Western African monsoon signal

395   and dinocyst assemblages is less evident during the recorded wetter interval ranging from 39

396   to 27.5 ka BP (Figure 6). Our dinocyst data would indeed suggest a better correlation with the

397   maximum of the Eastern African monsoon signal (Figure 6) while the Western one remained

398   weakened. This pattern is well correlated with pollen-inferred paleo precipitations data

399   extracted from Burundi mounts (Bonnefille and Chalié, 2000), which display higher

400   precipitations during this interval, also in accordance with strengthened Eastern African

401   monsoons (Figure 6).

402

403   ***5.2. Sub-orbital variations over the last 20 ka***

404   *5.2.1. The Last deglaciation*

405

406   <u>*The tropical response of Heinrich Stadial 1 (HS1)*</u>

407   Between 18 and 15.5 ka BP, thermophile and river-plume species abundances sharply dropped

408   while *O. centrocarpum* reached very high percentages (up to 50%) at that time (sub-

409   palynozone c1; Figure 7). Combined with low occurrences of *T. applanatum* (Figure 7), *O.*

410   *centrocarpum* here suggest significant SST cooling, probably induced by an intensification of

411   the BC activity in the area, and associated with enhanced upwelling cells activity. This

412   dinocyst pattern is consistent with previous observations that described a strong drought on

413   the African continent (Stager et al., 2002; Stager et al., 2011; Bouimetarhan et al., 2012;

414   Weldeab et al, 2012), as recorded through low precipitations (Bonnefille and Chalié, 2000;

415   Schefuss et al., 2005; Figure 6) associated with a continental and marine cooling ranging

416   between 1 and 2°C below LGM mean values (Mueller et al., 1998; Weldeab et al., 2007;

417   Powers et al., 2008; Weldeab et al., 2011; Shannon et al., 2012).

418   This cool and dry event appears synchronous with a massive advection of freshwater melting

419   that occurred in the North Atlantic Basin during Heinrich Stadial (HS) 1. The tropical

420   response of HS 1 would then consist in the southward shift of the TR (Arbuszewski et al.,

421   2013; McGee et al., 2014), involving a contraction of the latitudinal belts (Stager et al., 2011)

422   and weakened monsoons during this period. It is interesting to note that, while dinocysts

423   evidence a marked sea-surface cooling, isotopic signals from nearby core GeoB6518-1

424   (Schefuss et al., 2005; Figure 7) suggest a steady increase in tropical moisture all along HS1.

425   This implies a fundamental divergence between marine and continental compartments across

426   the Last Deglaciation.

427

428   *The equatorial signal of increasing deglacial warming at 15.5 ka BP*

429   Around 15.5-15 ka BP, the equatorial deglacial transition occurred in parallel with a global

430   warming (Syee Weldeab, 2005; Weijers et al., 2007; Leduc et al., 2010), linked with the

431   Northern Hemisphere July insolation increase. This resulted in a northward shift of the TR

432   (Arbuszewski et al., 2013; McGee et al., 2014) and thus strengthened monsoon activities.

433   Our dinocyst data also show a significant transition at around 15.5 ka BP (limit between

434   palynozones B and C; Figure 7) with the rapid increase of *Brigantedinium* spp. and

435   *Echinidinium* spp. percentages (Figure 7). Their modern distributions in the tropics are both

436   related to nutrient-enriched waters and, more specifically for *Echinidinium* spp., to high river-

437   discharges (Zonneveld et al., 2013). This is consistent with the strong increase of terrigenous

438   inputs observed at that time in the same study core (Bayon et al., 2012; Figure 7). The

439   equatorial species *O. aguinawense* also occurred shortly at around 15.5 ka BP (Figure 7),

18

440   suggesting a short high near-equatorial moisture event. *L. machaerophorum* abundances also

441   re-increased at 15.5 ka BP but remained low in comparison with glacial ones, suggesting a

442   specific switch in fluvial-sensitive dinocyst tracers between *L. machaerophorum* (glacial) and

443   *Echinidinium* spp.(across and after the Last Deglaciation).

444   Among the thermophile species, *Selenopemphix nephroides* and especially *Stelladinium reidii*

445   are the most obvious signals of the post 15.5 ka BP deglacial warming (Figure 7). Both

446   species are also considered as good tracers for high regimes of trophic conditions (Zonneveld

447   et al., 2013), in agreement with the recorded surface nutrient enrichment previously suggested

448   during this period (cf. *Brigantedinium* spp. and *Echinidinium* spp.). .

449

450   *The tropical response of the Younger Dryas (YD)*

451   Significant dinocyst changes occurred between around 13 and 11.5 ka BP in both dinocyst and

452   geochemical records (Figure 7). The significant drop of XRF Ti/Ca ratio evidences a reducing

453   of terrigenous inputs, while percentages of thermophile species *S. mirabilis*, *S. nephroides* and

454   *S. reidii* strongly decrease, then suggesting a significant cooling of surface waters in the study

455   area. The recorded cooling would be in agreement with the Younger Dryas (John Lowe and

456   Hoek, 2001) timing (Figure 7). However, high abundances of *Echinidinium* spp.and

457   *Brigantedinium* spp. during this interval suggest that nutrient-enriched river discharges still

458   occurred at that time (Figure 7). Our recorded tropical wetter conditions could be explained

459   by a suitable location of the TR above the Congo Basin, between Holocene and LGM mean

460   location (Arbuszewski et al., 2013; McGee et al., 2014). Furthermore, the weakening of the

461   deglacial sea-level rise during this period (Grant et al., 2012) and therefore the decrease of

462   associated continental shelf reworking (Marret et al., 2008) could explain the observed drop in

463   terrigenous inputs and the long-term decreasing trend of *Echinidinium* spp. (Figure 7). The

464   absence of *T. applanatum* during the tropical response of the YD would also suggest the

465   absence of upwelling cells in the study area (Figure 6). Nevertheless, high abundance of *S.*

466   *quanta* and *S. membranaceus* (Figures 5 and 7), generally well abundant in the vicinity of

467   seasonal upwelling cells (Marret and Zonneveld, 2003), may suggest the development of

468   seasonal coastal upwelling close to the study area, probably related to the suborbital-scale

469   northward shift of the ABF (Jansen et al., 1996).

470

471   *5.2.2 The Holocene*

472   The weak chrono-stratigraphic constraint of the Holocene (cf. Figure 2) leads to take great

473   caution in the interpretation of detailed specific events. However, some major subdivisions

474   (Early-, Mid-, and Late-Holocene) can be generally discussed (Figure 7).

475

476   *The Early Holocene and African Humid Period*

477   Across the Holocene, the African Humid Period (AHP) is a significantly warmer and wetter

478   period that occurred between around 14.5 and 5 ka BP (deMenocal et al., 2000; Shanahan et

479   al., 2015). At that time, the TR was characterized by a wider latitudinal extension up to

480   several degrees poleward (Stager et al., 2011; Arbuszewski et al., 2013; McGee et al., 2014).

481   Previous dinocyst studies, showed that the AHP was characterized by the gradual bloom of

482   thermophile (*S. mirabilis*) and low-salinity (*O. aguinawense*) species, induced by

483   strengthened river discharges from the beginning of the Holocene (Dupont and Behling, 2006;

484   Kim et al., 2010; Marret et al., 2013).

485   Similarly to these published data, our record also evidences a strengthening of nutrient-

486   enriched river discharges from the onset of the last deglaciation (Figure 7; cf. subchapter

487   5.2.1). However significant occurrences of *O. aguinawense* between around 11 and 2 ka BP

488   (Figure 7) delimit the effective wettest period also characterized by the highest abundances of

489   both mesotrophic and eutrophic thermophile species (Figure 7). High SST recorded at the

490   beginning of the Holocene are also well correlated with alkenone SST reconstructions from

491   core GeoB6518 (Schefuß et al., 2005) synchronously with the Early Holocene timing (Figure

492   7). It is also interesting to note that, during this Holocene climatic optimum, our dinocyst data

493   show a sharp drop of *Echinidinium* abundance between 8 and 7 ka BP, synchronously with a

494   drop of thermophile species (Figure 7). This could suggest a thousand years-long cooler and

495   drier event that occurred during the Early and Mid-Holocene transition (Walker et al., 2012).

496

497   *The Mid-Holocene transition and the end of African Humid Period*

498   The timing of the AHP termination significantly changes according to authors and study sites

499   (Figure 7), i.e around 2.5 ka BP (Kröpelin et al., 2008; Lézine et al., 2013; Shanahan et al.,

500   2012; Lebamba et al., 2012), 4 ka BP (deMenocal et al., 2000; Hély et al., 2009; Tierney and

501   deMenocal, 2013; Shanahan et al., 2015), or even earlier around 5.3 ka BP (Lézine et al.,

502   2005). The length of the AHP termination also changes significantly, from a few centuries to a

503   few thousand years (Figure 7) according to the references mentioned above.

504   In our data, we observe two abrupt degradation steps during a millennial-scale heat and

505   moisture mitigation. The first mitigation occurred abruptly between 7 and 6 ka BP (transition

506   between sub-palynozones b1 and b2), illustrated by the sharp drop of heterotrophic taxa

507   percentages, especially *Brigantedinium* species, *S. reidii* and *S. nephroides* (Figure 7), in

508   parallel with high abundances of *O. centrocarpum*. This suggests an environmental change

509   from eutrophic to lower nutrient-enriched surface waters, probably allowing the observed

510   development of mesotrophic taxa, such as *S. mirabilis* (Figure 7). This mitigation does not

511   appear as a dry event, due to: i) the persistence of high *Echinidinium* spp. abundances, with

512   however a long-term decreasing trend obvious since 15.5 ka BP (Figure 7) and ii) the

513   persistence of *O. aguinawense* (today related to near-equatorial hydrological conditions)

514   which reached its highest abundances during this interval (sub-palynozone b1, Figure 7).

515   The second mitigation occurred abruptly between 4 and 3.5 ka BP (transition between

516   palynozones A and B; Figure 7), as displayed by a general drop of both heterotrophic and

517   thermophile cyst percentages, while *O. centrocarpum* rapidly became the major dinocyst

518   species (Figure 7). As we discussed above from crossed information related to total dinocyst

519   concentrations and community indexes (dominance *versus* diversity; cf. Section 4.1 and

520   Figure 3), the interval ranging from 4 to 2.5 ka BP (sub-palynozone a2; Figure 7) is probably

521   characterized by massive advection of *O. centrocarpum* cysts. However, removing *O.*

522   *centrocarpum* from abundance calculations of other taxa will not remove the observed shift

523   discussed above for heterotrophic and thermophile dinocysts and clearly related the 4-3.5 ka

524   BP period.

525

526   *The Late Holocene*

527   Right after 3.5 ka BP the interval appears to be one of the coolest and driest periods ever

528   recorded in core KZAI-01, as it was observed elsewhere in tropical Atlantic latitudes (Marret

529   et al., 2006). This could be the consequence of a strengthened advection of the BC northward,

530   maybe also related to a 4° northward shift of the ABF, well recorded during the Mid to Late

531   Holocene (Jansen et al., 1996).

532

533   Finally, since 2.5 ka BP (subpalynozone a1), a recovery of *L. machaerophorum* and

534   *Echinidinium* spp.percentages is observed in parallel with low occurrences of *O. aguinawense*

535   (Figures 5 and 7), suggesting a slight re-increase of wetter conditions. However, despite the

536   general warming observed in several SST reconstructions in tropical studies over this period

537   (Schefuß et al., 2005; Weldeab et al., 2005; Dyez et al., 2014), all thermophile cyst

538   percentages remain zero or very low (Figure 7). The recovery of wetter conditions may be

539   explained by the optimum of the precession index reached around 3 ka BP (Figure 6), which

540   implies the correspondence between austral summer and Earth perihelion and allows the

541   establishment of wetter and warmer conditions in the Southern Hemisphere.

542   The Holocene as recorded in core KZAI-01 can be then divided into three major periods. The

543   earliest interval (11-6.5 ka BP) is also the warmest and wettest period, followed between 6.5

544   and 4 ka BP by a mitigated warm and humid period characterized by the progressive recovery

545   of the BC advection. Finally, after 4 ka BP, a major long-term cooling and drying period is

546   gradually pondered by a progressive recovery of river discharges in the study area since 2.5

547   ka BP.

548

549   **6. CONCLUSION**

550   Dinocyst assemblage analysis conducted on core KZAI-01 has permitted an investigation of

551   land-sea-atmosphere linkages off the Congo River mouth over the last 44 ka. Our dinocyst

552   data evidence a great influence of nutrient-rich river discharges induced by the Tropical

553   Rainbelt latitudinal migrations, themselves forced by different orbital configurations, and

554   especially regarding the combination "precession minima - obliquity maxima". Furthermore,

555   while most of tropical studies describe the LGM as a "cold and dry" period in the tropics,

556   dinocyst assemblages evidence here a slightly warmer and wetter period than it was expected.

557   The LGM appears to be a complex period characterized by a southward latitudinal shift of the

558   monsoonal belt and of warm surface waters, bringing heat and moisture. This illustrates a

559   complex scheme that would deserve model simulations and unravelling precise underlying

560   mechanisms and impacts that occurred across this specific climate interval.

561   This high-resolution study has also permitted to discriminate major climatic periods of the

562   Last Deglaciation in good correspondence with Northern Hemisphere high latitude millennial-

563   scale oscillations. We also discussed the timing of the equatorial response of the African

564   Humid Period and the two-steps mitigation of heat and moisture conditions in the study area.

565 Further work will involve a regional-scale study including other dinocyst records to

566 reconstruct sea-surface environments in relationship with Tropical Rainbelt latitudinal shifts

567 along the African Western façade, as well as model-data inter-comparisons for different

568 snapshots across the last glacial, deglacial and Holocene periods.

569

570 **7. ACKNOWLEDGEMENTS**

575

576

Biogeosciences
Open Access
Discussions
EGU

577 **8. REFERENCES**

578 Anhuf, D., Ledru, M.-P., Behling, H., Da Cruz Jr., F. W., Cordeiro, R. C., Van der Hammen,
579 T., Karmann, I., Marengo, J. A., De Oliveira, P. E., Pessenda, L., Siffedine, A., Albuquerque,
580 A. L. and Da Silva Dias, P. L.: Paleo-environmental change in Amazonian and African
581 rainforest during the LGM, Palaeogeography, Palaeoclimatology, Palaeoecology, 239(3–4),
582 510–527, doi:10.1016/j.palaeo.2006.01.017, 2006.

583 Anka, Z., Séranne, M., Lopez, M., Scheck-Wenderoth, M. and Savoye, B.: The long-term
584 evolution of the Congo deep-sea fan: A basin-wide view of the interaction between a giant
585 submarine fan and a mature passive margin (ZaiAngo project), Tectonophysics, 470(1–2), 42–
586 56, doi:10.1016/j.tecto.2008.04.009, 2009.

587 Arbuszewski, J. A., deMenocal, P. B., Cléroux, C., Bradtmiller, L. and Mix, A.: Meridional
588 shifts of the Atlantic intertropical convergence zone since the Last Glacial Maximum, Nature
589 Geosci, 6(11), 959–962, doi:10.1038/ngeo1961, 2013.

590 Babonneau, N., Savoye, B., Cremer, M. and Klein, B.: Morphology and architecture of the
591 present canyon and channel system of the Zaire deep-sea fan, Marine and Petroleum Geology,
592 19(4), 445–467, doi:10.1016/S0264-8172(02)00009-0, 2002.

593 Bayon, G., Dennielou, B., Etoubleau, J., Ponzevera, E., Toucanne, S. and Bermell, S.:
594 Intensifying Weathering and Land Use in Iron Age Central Africa, Science, 335(6073), 1219–
595 1222, doi:10.1126/science.1215400, 2012.

596 Berger, A. and Loutre, M. F.: Insolation values for the climate of the last 10 million years,
597 Quaternary Science Reviews, 10(4), 297–317, doi:10.1016/0277-3791(91)90033-Q, 1991.

598 Bonnefille, R. and Chalié, F.: Pollen-inferred precipitation time-series from equatorial
599 mountains, Africa, the last 40 kyr BP, Global and Planetary Change, 26(1–3), 25–50,
600 doi:10.1016/S0921-8181(00)00032-1, 2000.

601 Bosmans, J. H. C., Hilgen, F. J., Tuenter, E. and Lourens, L. J.: Obliquity forcing of low-
602 latitude climate, Clim. Past, 11(10), 1335–1346, doi:10.5194/cp-11-1335-2015, 2015.

603 Bouimetarhan, I., Prange, M., Schefuß, E., Dupont, L., Lippold, J., Mulitza, S. and
604 Zonneveld, K.: Sahel megadrought during Heinrich Stadial 1: evidence for a three-phase
605 evolution of the low- and mid-level West African wind system, Quaternary Science Reviews,
606 58, 66–76, doi:10.1016/j.quascirev.2012.10.015, 2012.

607 Bultot, F.: Atlas climatique du bassin congolais, I.N.É.A.C., 1971.

608 Collier, A. B. and Hughes, A. R. W.: Lightning and the African ITCZ, Journal of Atmospheric
609 and Solar-Terrestrial Physics, 73(16), 2392–2398, doi:10.1016/j.jastp.2011.08.010, 2011.

610 da Cunha, L. C. and Buitenhuis, E. T.: Riverine influence on the tropical Atlantic Ocean
611 biogeochemistry, Biogeosciences, 10(10), 6357–6373, doi:10.5194/bg-10-6357-2013, 2013.

612 deMenocal, P., Ortiz, J., Guilderson, T., Adkins, J., Sarnthein, M., Baker, L. and Yarusinsky,
613 M.: Abrupt onset and termination of the African Humid Period:: rapid climate responses to
614 gradual insolation forcing, Quaternary Science Reviews, 19(1–5), 347–361,
615 doi:10.1016/S0277-3791(99)00081-5, 2000.

616   deMenocal, P. B., Ruddiman, W. F. and Pokras, E. M.: Influences of High- and Low-Latitude
617   Processes on African Terrestrial Climate: Pleistocene Eolian Records from Equatorial Atlantic
618   Ocean Drilling Program Site 663, Paleoceanography, 8(2), 209–242, doi:10.1029/93PA02688,
619   1993.

620   Droz, L., Marsset, T., Ondréas, H., Lopez, M., Savoye, B. and Spy-Anderson, F.-L.:
621   Architecture of an active mud-rich turbidite system: The Zaire Fan (Congo–Angola margin
622   southeast Atlantic) Results from ZaïAngo 1 and 2 cruises, AAPG Bulletin, 87(7), 1145–1168,
623   doi:10.1306/03070300013, 2003.

624   Dupont, L. and Behling, H.: Land–sea linkages during deglaciation: High-resolution records
625   from the eastern Atlantic off the coast of Namibia and Angola (ODP site 1078), Quaternary
626   International, 148(1), 19–28, doi:10.1016/j.quaint.2005.11.004, 2006.

627   Dupont, L. M., Marret, F. and Winn, K.: Land-sea correlation by means of terrestrial and
628   marine palynomorphs from the equatorial East Atlantic: phasing of SE trade winds and the
629   oceanic productivity, Palaeogeography, Palaeoclimatology, Palaeoecology, 142(1–2), 51–84,
630   doi:10.1016/S0031-0182(97)00146-6, 1998.

631   F Fatela, R. T.: Confidence limits of species proportions in microfossil assemblages, Marine
632   Micropaleontology, 45(2), 169–174, doi:10.1016/S0377-8398(02)00021-X, 2002.

633   Gordon, A. L., Bosley, K. T. and Aikman III, F.: Tropical atlantic water within the Benguela
634   upwelling system at 27°S, Deep Sea Research Part I: Oceanographic Research Papers, 42(1),
635   1–12, doi:10.1016/0967-0637(94)00032-N, 1995.

636   Hansen, M. C., Potapov, P. V., Moore, R., Hancher, M., Turubanova, S. A., Tyukavina, A.,
637   Thau, D., Stehman, S. V., Goetz, S. J., Loveland, T. R., Kommareddy, A., Egorov, A., Chini,
638   L., Justice, C. O. and Townshend, J. R. G.: High-Resolution Global Maps of 21st-Century
639   Forest Cover Change, Science, 342(6160), 850–853, doi:10.1126/science.1244693, 2013.

640   Heezen, B. C. and Hollister, C.: Deep-sea current evidence from abyssal sediments, Marine
641   Geology, 1(2), 141–174, doi:10.1016/0025-3227(64)90012-X, 1964.

642   Hély, C., Braconnot, P., Watrin, J. and Zheng, W.: Climate and vegetation: Simulating the
643   African humid period, Comptes Rendus Geoscience, 341(8–9), 671–688,
644   doi:10.1016/j.crte.2009.07.002, 2009.

645   Hirahara, S., Ishii, M. and Fukuda, Y.: Centennial-Scale Sea Surface Temperature Analysis
646   and Its Uncertainty, J. Climate, 27(1), 57–75, doi:10.1175/JCLI-D-12-00837.1, 2013.

647   Holzwarth, U., Esper, O. and Zonneveld, K.: Distribution of organic-walled dinoflagellate
648   cysts in shelf surface sediments of the Benguela upwelling system in relationship to
649   environmental conditions, Marine Micropaleontology, 64(1–2), 91–119,
650   doi:10.1016/j.marmicro.2007.04.001, 2007.

651   Hsu, C.-P. F. and Wallace, J. M.: The Global Distribution of the Annual and Semiannual
652   Cycles in Precipitation, Mon. Wea. Rev., 104(9), 1093–1101, doi:10.1175/1520-
653   0493(1976)104<1093:TGDOTA>2.0.CO;2, 1976.

654   Jansen, J. H. F., Ufkes, E. and Schneider, R. R.: Late Quaternary Movements of the Angola-
655   Benguela Front, SE Atlantic, and Implications for Advection in the Equatorial Ocean, in The

656   South Atlantic, pp. 553–575, Springer Berlin Heidelberg. [online] Available from:
657   http://scdproxy.univ-brest.fr:2068/chapter/10.1007/978-3-642-80353-6_28 (Accessed 28
658   October 2014), 1996.

659   John Lowe, J. and Hoek, W. Z.: Inter-regional correlation of palaeoclimatic records for the
660   Last Glacial–Interglacial Transition: a protocol for improved precision recommended by the
661   INTIMATE project group, Quaternary Science Reviews, 20(11), 1175–1187,
662   doi:10.1016/S0277-3791(00)00183-9, 2001.

663   Khripounoff, A., Vangriesheim, A., Babonneau, N., Crassous, P., Dennielou, B. and Savoye,
664   B.: Direct observation of intense turbidity current activity in the Zaire submarine valley at
665   4000 m water depth, Marine Geology, 194(3–4), 151–158, doi:10.1016/S0025-
666   3227(02)00677-1, 2003.

667   Kim, S.-Y., Scourse, J., Marret, F. and Lim, D.-I.: A 26,000-year integrated record of marine
668   and terrestrial environmental change off Gabon, west equatorial Africa, Palaeogeography,
669   Palaeoclimatology, Palaeoecology, 297(2), 428–438, doi:10.1016/j.palaeo.2010.08.026, 2010.

670   Kröpelin, S., Verschuren, D., Lézine, A.-M., Eggermont, H., Cocquyt, C., Francus, P., Cazet,
671   J.-P., Fagot, M., Rumes, B., Russell, J. M., Darius, F., Conley, D. J., Schuster, M.,
672   Suchodoletz, H. von and Engstrom, D. R.: Climate-Driven Ecosystem Succession in the
673   Sahara: The Past 6000 Years, Science, 320(5877), 765–768, doi:10.1126/science.1154913,
674   2008.

675   Lass, H. U. and Mohrholz, V.: On the interaction between the subtropical gyre and the
676   Subtropical Cell on the shelf of the SE Atlantic, Journal of Marine Systems, 74(1–2), 1–43,
677   doi:10.1016/j.jmarsys.2007.09.008, 2008.

678   Lebamba, J., Vincens, A. and Maley, J.: Pollen, vegetation change and climate at Lake
679   Barombi Mbo (Cameroon) during the last ca. 33 000 cal yr BP : a numerical approach,
680   Climate of the Past, 8(1), 59–78, doi:10.5194/cp-8-59-2012, 2012.

681   Leduc, G., Schneider, R., Kim, J.-H. and Lohmann, G.: Holocene and Eemian sea surface
682   temperature trends as revealed by alkenone and Mg/Ca paleothermometry, Quaternary
683   Science Reviews, 29(7–8), 989–1004, doi:10.1016/j.quascirev.2010.01.004, 2010.

684   Lempicka, M.: Lempicka (Magdalena), Bilan hydrique du bassin du fleuve Zaïre. 1ère Partie :
685   Ecoulement du bassin 1950-1959. Kinshasa : Office National de la Recherche et du
686   Développement (ONRD), 1971, 147 p., Office National de la Recherche et du Développement
687   (ONRD), Kinshasa., 1971.

688   Leroux, M.: The Meteorology and Climate of Tropical Africa | Marcel Leroux | Springer.
689   [online] Available from: http://www.springer.com/us/book/9783540426363 (Accessed 14
690   December 2015), 2001.

691   Lézine, A.-M., Duplessy, J.-C. and Cazet, J.-P.: West African monsoon variability during the
692   last deglaciation and the Holocene: Evidence from fresh water algae, pollen and isotope data
693   from core KW31, Gulf of Guinea, Palaeogeography, Palaeoclimatology, Palaeoecology,
694   219(3–4), 225–237, doi:10.1016/j.palaeo.2004.12.027, 2005.

695   Lézine, A.-M., Holl, A. F.-C., Lebamba, J., Vincens, A., Assi-Khaudjis, C., Février, L. and
696   Sultan, É.: Temporal relationship between Holocene human occupation and vegetation change

along the northwestern margin of the Central African rainforest, Comptes Rendus Geoscience, 345(7–8), 327–335, doi:10.1016/j.crte.2013.03.001, 2013.

Loomis, S. E., Russell, J. M., Ladd, B., Street-Perrott, F. A. and Sinninghe Damsté, J. S.: Calibration and application of the branched GDGT temperature proxy on East African lake sediments, Earth and Planetary Science Letters, 357–358, 277–288, doi:10.1016/j.epsl.2012.09.031, 2012.

Marret, F. and Kim, S.-Y.: Operculodinium aguinawense sp. nov., A Dinoflagellate Cyst from the Late Pleistocene and Recent Sediments of the East Equatorial Atlantic Ocean, Palynology, 33(1), 125–139, doi:10.2113/gspalynol.33.1.125, 2009.

Marret, F. and Zonneveld, K. A. F.: Atlas of modern organic-walled dinoflagellate cyst distribution, Review of Palaeobotany and Palynology, 125(1–2), 1–200, doi:10.1016/S0034-6667(02)00229-4, 2003.

Marret, F., Maley, J. and Scourse, J.: Climatic instability in west equatorial Africa during the Mid- and Late Holocene, Quaternary International, 150(1), 71–81, doi:10.1016/j.quaint.2006.01.008, 2006.

Marret, F., Scourse, J., Kennedy, H., Ufkes, E. and Jansen, J. H. F.: Marine production in the Congo-influenced SE Atlantic over the past 30,000 years: A novel dinoflagellate-cyst based transfer function approach, Marine Micropaleontology, 68(1–2), 198–222, doi:10.1016/j.marmicro.2008.01.004, 2008.

Marret, F., Kim, S.-Y. and Scourse, J.: A 30,000 yr record of land–ocean interaction in the eastern Gulf of Guinea, Quaternary Research, 80(1), 1–8, doi:10.1016/j.yqres.2013.04.003, 2013.

McGee, D., Donohoe, A., Marshall, J. and Ferreira, D.: Changes in ITCZ location and cross-equatorial heat transport at the Last Glacial Maximum, Heinrich Stadial 1, and the mid-Holocene, Earth and Planetary Science Letters, 390, 69–79, doi:10.1016/j.epsl.2013.12.043, 2014.

Merlis, T. M., Schneider, T., Bordoni, S. and Eisenman, I.: The Tropical Precipitation Response to Orbital Precession, J. Climate, 26(6), 2010–2021, doi:10.1175/JCLI-D-12-00186.1, 2012.

Minze Stuiver, P. J. R.: Extended 14C Database and Revised CALIB Radiocarbon Calibration Program (Version 5.0), Radiocarbon, 35, 1992.

Mix, A. C., Bard, E. and Schneider, R.: Environmental processes of the ice age: land, oceans, glaciers (EPILOG), Quaternary Science Reviews, 20(4), 627–657, doi:10.1016/S0277-3791(00)00145-1, 2001.

Nicholson, S. E.: A revised picture of the structure of the "monsoon" and land ITCZ over West Africa, Clim Dyn, 32(7–8), 1155–1171, doi:10.1007/s00382-008-0514-3, 2009.

Picot, M., Droz, L., Marsset, T., Dennielou, B. and Bez, M.: Controls on turbidite sedimentation: Insights from a quantitative approach of submarine channel and lobe architecture (Late Quaternary Congo Fan), Marine and Petroleum Geology, 72, 423–446, doi:10.1016/j.marpetgeo.2016.02.004, 2016.

Biogeosciences
Discussions

Open Access

EGU

737 Powers, L. A., Johnson, T. C., Werne, J. P., Castañeda, I. S., Hopmans, E. C., Sinninghe
738 Damsté, J. S. and Schouten, S.: Large temperature variability in the southern African tropics
739 since the Last Glacial Maximum, Geophys. Res. Lett., 32(8), L08706,
740 doi:10.1029/2004GL022014, 2005.

741 Prance, G. T.: The vegetation of Africa. by F. White, Brittonia, 36(3), 273–273,
742 doi:10.2307/2806524, 1984.

743 Reimer, P.: IntCal13 and Marine13 Radiocarbon Age Calibration Curves 0–50,000 Years cal
744 BP, Radiocarbon, 55(4), 1869–1887, doi:10.2458/azu_js_rc.55.16947, 2013.

745 Savoye, B.: Zaiango 1 cruise report mission, , doi:10.17600/98010100, 1998.

746 Savoye, B., Cochonat, P., Apprioual, R., Bain, O., Baltzer, A., Bellec, V., Beuzart, P.,
747 Bourillet, J.-F., Cagna, R., Cremer, M., Crusson, A., Dennielou, B., Diebler, D., Droz, L.,
748 Ennes, J.-C., Floch, G., Guiomar, M., Harmegnies, F., Kerbrat, R., Klein, B., Kuhn, H.,
749 Landuré, J.-Y., Lasnier, C., Le Drezen, E., Le Formal, J.-P., Lopez, M., Loubrieu, B., Marsset,
750 T., Migeon, S., Normand, A., Nouzé, H., Ondréas, H., Pelleau, P., Saget, P., Séranne, M.,
751 Sibuet, J.-C., Tofani, R. and Voisset, M.: Structure et évolution récente de l'éventail
752 turbiditique du Zaïre : premiers résultats scientifiques des missions d'exploration Zaïango1 &
753 2 (marge Congo–Angola), Comptes Rendus de l'Académie des Sciences - Series IIA - Earth
754 and Planetary Science, 331(3), 211–220, doi:10.1016/S1251-8050(00)01385-9, 2000.

755 Savoye, B., Babonneau, N., Dennielou, B. and Bez, M.: Geological overview of the Angola–
756 Congo margin, the Congo deep-sea fan and its submarine valleys, Deep Sea Research Part II:
757 Topical Studies in Oceanography, 56(23), 2169–2182, doi:10.1016/j.dsr2.2009.04.001, 2009.

758 Schefuß, E., Schouten, S. and Schneider, R. R.: Climatic controls on central African
759 hydrology during the past 20,000 years, Nature, 437(7061), 1003–1006,
760 doi:10.1038/nature03945, 2005.

761 Schneider, R. R., Price, B., Müller, P. J., Kroon, D. and Alexander, I.: Monsoon related
762 variations in Zaire (Congo) sediment load and influence of fluvial silicate supply on marine
763 productivity in the east equatorial Atlantic during the last 200,000 years, Paleoceanography,
764 12(3), 463–481, doi:10.1029/96PA03640, 1997.

765 Shakun, J. D. and Carlson, A. E.: A global perspective on Last Glacial Maximum to Holocene
766 climate change, Quaternary Science Reviews, 29(15–16), 1801–1816,
767 doi:10.1016/j.quascirev.2010.03.016, 2010.

768 Shanahan, T. M., Beck, J. W., Overpeck, J. T., McKay, N. P., Pigati, J. S., Peck, J. A., Scholz,
769 C. A., Heil Jr., C. W. and King, J.: Late Quaternary sedimentological and climate changes at
770 Lake Bosumtwi Ghana: New constraints from laminae analysis and radiocarbon age
771 modeling, Palaeogeography, Palaeoclimatology, Palaeoecology, 361–362, 49–60,
772 doi:10.1016/j.palaeo.2012.08.001, 2012.

773 Shanahan, T. M., McKay, N. P., Hughen, K. A., Overpeck, J. T., Otto-Bliesner, B., Heil, C. W.,
774 King, J., Scholz, C. A. and Peck, J.: The time-transgressive termination of the African Humid
775 Period, Nature Geosci, 8(2), 140–144, doi:10.1038/ngeo2329, 2015.

776 Shi, N., Dupont, L. M., Beug, H.-J. and Schneider, R.: Vegetation and climate changes during
777 the last 21 000 years in S.W. Africa based on a marine pollen record, Veget Hist Archaebot,

Biogeosciences
Open Access
Discussions
EGU

778   7(3), 127–140, doi:10.1007/BF01374001, 1998.

779   Stager, J. C., Ryves, D. B., Chase, B. M. and Pausata, F. S. R.: Catastrophic Drought in the
780   Afro-Asian Monsoon Region During Heinrich Event 1, Science, 331(6022), 1299–1302,
781   doi:10.1126/science.1198322, 2011.

782   Syee Weldeab, R. R. S.: Holocene African droughts relate to eastern equatorial Atlantic
783   cooling. Geology, Geology, 33(12), doi:10.1130/G21874.1, 2005.

784   Tierney, J. E. and deMenocal, P. B.: Abrupt Shifts in Horn of Africa Hydroclimate Since the
785   Last Glacial Maximum, Science, 342(6160), 843–846, doi:10.1126/science.1240411, 2013.

786   Tierney, J. E., Russell, J. M., Sinninghe Damsté, J. S., Huang, Y. and Verschuren, D.: Late
787   Quaternary behavior of the East African monsoon and the importance of the Congo Air
788   Boundary, Quaternary Science Reviews, 30(7–8), 798–807,
789   doi:10.1016/j.quascirev.2011.01.017, 2011.

790   Tuenter, E., Weber, S. L., Hilgen, F. J. and Lourens, L. J.: The response of the African summer
791   monsoon to remote and local forcing due to precession and obliquity, Global and Planetary
792   Change, 36(4), 219–235, doi:10.1016/S0921-8181(02)00196-0, 2003.

793   Voituriez, B.: Les sous-courants équatoriaux nord et sud et la formation des dômes thermiques
794   tropicaux, Oceanologica Acta, 4(4), 497–506, 1981.

795   Walker, M. J. C., Berkelhammer, M., Björck, S., Cwynar, L. C., Fisher, D. A., Long, A. J.,
796   Lowe, J. J., Newnham, R. M., Rasmussen, S. O. and Weiss, H.: Formal subdivision of the
797   Holocene Series/Epoch: a Discussion Paper by a Working Group of INTIMATE (Integration
798   of ice-core, marine and terrestrial records) and the Subcommission on Quaternary
799   Stratigraphy (International Commission on Stratigraphy), J. Quaternary Sci., 27(7), 649–659,
800   doi:10.1002/jqs.2565, 2012.

801   Weijers, J. W. H., Schefuß, E., Schouten, S. and Damsté, J. S. S.: Coupled Thermal and
802   Hydrological Evolution of Tropical Africa over the Last Deglaciation, Science, 315(5819),
803   1701–1704, doi:10.1126/science.1138131, 2007.

804   Zarriess, M. and Mackensen, A.: The tropical rainbelt and productivity changes off northwest
805   Africa: A 31,000-year high-resolution record, Marine Micropaleontology, 76(3–4), 76–91,
806   doi:10.1016/j.marmicro.2010.06.001, 2010.

807   Zonneveld, K. A. F., Marret, F., Versteegh, G. J. M., Bogus, K., Bonnet, S., Bouimetarhan, I.,
808   Crouch, E., de Vernal, A., Elshanawany, R., Edwards, L., Esper, O., Forke, S., Grøsfjeld, K.,
809   Henry, M., Holzwarth, U., Kielt, J.-F., Kim, S.-Y., Ladouceur, S., Ledu, D., Chen, L.,
810   Limoges, A., Londeix, L., Lu, S.-H., Mahmoud, M. S., Marino, G., Matsouka, K.,
811   Matthiessen, J., Mildenhal, D. C., Mudie, P., Neil, H. L., Pospelova, V., Qi, Y., Radi, T.,
812   Richerol, T., Rochon, A., Sangiorgi, F., Solignac, S., Turon, J.-L., Verleye, T., Wang, Y.,
813   Wang, Z. and Young, M.: Atlas of modern dinoflagellate cyst distribution based on 2405 data
814   points, Review of Palaeobotany and Palynology, 191, 1–197,
815   doi:10.1016/j.revpalbo.2012.08.003, 2013.

816

817

9. TABLE AND FIGURE CAPTIONS

9.1. Table caption

Table 1 : Inventory of all dates obtained in the core KZAI-01 : 14C AMS datations obtained from carbonate materials (Bayon et al., 2012), 14C AMS datations obtained from bulk organic matter (Bayon et al., 2012) and finally dates obtained from tuning with core GeoB6518-1 (Schefuß et al., 2005; Bayon et al., 2012). Rejected dates are displayed in red.

9.2. Figure captions

Figure 1: Map showing locations of KZAI-01 core and other cores mentioned in the text: GeoB6518 (Schefuß et al., 2005; Bayon et al., 2012), GeoB1008 (Schneider et al., 1997) and GITANGA2 (Bonnefille and Chalié, 2000). The general pattern of present-day surface ocean currents of the adjacent Atlantic Ocean is extracted from Lass and Mohrholz (2008) and includes: the Guinea Current (GC), the northern (nSEC), equatorial (eSEC), central (cSEC), and southern (sSEC) South Equatorial Current, the Angola Current (AC), the Angola-Benguela Front (ABF), the Benguela Current (BC) and the Agulhas Current (AgC). Orange lines indicate warm currents and blue lines cold currents. Green zones correspond to upwelling zone (BUS : Benguela upwelling system) and oceanic domes (AD : Angola Dome, ED : Equatorial Dome; Voituriez, 1981; Lass and Mohrholz, 2008). Black dashed line display the mean location of the ITCZ during July and January (Collier and Hughes, 2011). Red 5°C-interval isolines correspond to annual mean SST (Hirahara et al., 2013). Vegetation covering (in % per surface unity) is extracted from (Hansen et al., 2013) dataset.

Figure 2: Age model established on linear regression calculated from AMS ^{14}C datations on carbonate (red squares; cf. Table 1). Blue squares correspond to ^{14}C datations extracted from organic matter (Bayon et al., 2012), not taken into account for the age model. Green squares correspond to dates obtained by tuning with core GeoB6518, on the basis on similar trend observed in Ti / Ca XRF ratios extracted from respective cores. Grey band corresponds to the range error of calibrated dates, and purple lines correspond to the sedimentation rates (cm/ka).

Figure 3: Comparisons between total dinocyst concentration in the sediment (cysts / cm^3), the proportion of non-heterotrophic taxa concentration in the whole assemblage and the dominant species carrying this concentration, i.e *Lingulodinium machaerophorum and Operculodinium centrocarpum*. The same approach is applied for heterotrophic taxa, with the comparison between total heterotrophic concentrations in the sediment in the view of heterotrophic dominant species concentration, i.e *Brigantedinium* spp.and *Echinidinium* spp. The cited dominant species abundances are illustrated in cumulated percentages. To discuss the relationship between primary productivity, dinocysts concentrations and terrigenous dilution, the Ti/Ca XRF ratio of the core KZAI-01 is displayed, in addition with biogenic silica and total organic matter signals extracted from core GeoB1008 (Schneider et al., 1997). We added the specific diversity and dominance index to discuss the potential advection of allogeneic dinocysts in the study. Red dashed lines correspond to major transitions in total dinocysts concentration in the view of known major environmental shifts. Major palynozones (ABCDE) boundaries are established on the basis of major dinocysts concentration transition periods.

Biogeosciences
Discussions

Open Access

EGU

863 **Figure 4**: Detailed non-heterotrophic major species abundances in view of total dinocysts in
864 the sediment (cysts/cm^3). Some species have been grouped, such as *Spiniferites ramosus* and
865 *Spiniferites bulloides*, grouped into *Spiniferites ramosus*, and *Nematosphaeropsis labyrinthus*
866 grouped with *Nematosphaeropsis lemniscata*. Palynozones (A to E) have been established
867 according to the major dinocyst variations in absolute concentrations and relative abundances,
868 with minor subdivisions (Ax-Ex). Species are displayed here and classified according to
869 observed temporal successions, underlined by black arrows. Black arrows represent temporal
870 successions between species abundances.
871

872 **Figure 5**: Detailed heterotrophic taxa abundances in parallel with abundances of total
873 heterotrophic taxa and heterotrophic concentrations in cysts/cm^3. Some species have been
874 grouped, such as: *Echinidinium* spp.(*E. aculeatum, E. delicatum, E. granulatum* and *E.*
875 *transparentum*). *Lingulodinium machaerophorum* is displayed here with *Echinidinium*
876 spp.regarding their river-plume affinity. Palynozones (A to E) have been established
877 according to the major dinocyst variations in absolute concentrations and relative abundances,
878 with minor subdivisions (Ax-Ex). Heterotrophic species are displayed here and classified
879 according to observed temporal successions, underlined by black arrows. Black arrows
880 represent temporal successions between species abundances.
881

882 **Figure 6**: Comparison between total heterotrophic abundance and upwelling activity
883 displayed by *Trinovantedinium applanatum* (Marret & Zonneveld, 2003). Congo River
884 discharges are displayed on KZAI-01 core by river-plume sensitive species *Echinidinium* spp.
885 and *Lingulodinium machaerophorum,* Coenobia of *Pediastrum* and terrigenous inputs (Ti/Ca
886 XRF ratio, quantitative measurements of major elements Al/K and Al/Si; Bayon et al., 2012).
887 Relations between river discharges and paleomonsoon activity are displayed through rainfall
888 anomalies in Burundi mounts (Bonnefille & Chalié, 2000: the threshold with positive
889 anomalies in green and negative anomalies in orange is calculated from mean glacial values)
890 and regional-scale monsoon reconstructions (Western and Eastern African Monsoon; Caley et
891 al., 2011: maximal monsoon regimes are underlined in green). Orbital parameters such as
892 Obliquity and Precession (Berger and Loutre, 1991) are also displayed with precession
893 minima highlighted in green, and obliquity maxima highlighted in green. Green bands
894 correspond to major orbital-scale moisture conditions. dD on Alkane C29 from core
895 GeoB6518 is displayed in red with pollen-inferred paleo precipitation reconstructions.
896

897 **Figure 7:** Temporal focus on the last 20 ka BP. Sea-surface Temperature changes are
898 discussed with major dinocyst species, classified according their trophic affinity: *Spiniferites*
899 *mirabilis, Spiniferites membranaceus, Selenopemphix nephroides* and *Stelladinium reidii*.
900 Sea-surface salinities changes are discussed with: sum of Echinidinium species,
901 Operculodinium aguinawense, Lingulodinium machaerophorum, in addition with stable
902 isotopic signal from core GeoB6518-1 (Schefuss et al., 2005). Upwelling activity and
903 Benguela advection are discussed with *Trinovantedinium applanatum* and *Operculodinium*
904 *centrocarpum* respectively, and marine food abundance with *Brigantedinium* spp. Ti/Ca XRF
905 ratio of core KZAI-01 represents past terrigenous supplies. d18O GICC05 is displayed here
906 (Svensson et al., 2008) with the Deglaciation-Holocene subdivisions (Walker et al., 2012) :
907 Last Glacial Maximum (LGM), Heinrich Stadial 1 (HS1), Bølling-Allerød (B/A), Younger
908 Dryas (YD), Early Holocene (EH), Mid-Holocene (MH) and Late Holocene (LH). Blue bands
909 correspond to cold and dry events recorded with dinocyst assemblages. African Humid Period
910 (AHP) terminations are also depicted in the figure according to literature (orange bars) :

911 1°(Kröpelin et al., 2008), 2° (Shanahan et al., 2015), 3° (Hély et al., 2009), 4°(Lézine et al.,
912 2005), 5°(Lebamba et al., 2012), 6°(Lézine et al., 2013), 7°(Tierney and deMenocal, 2013),
913 8°(Shanahan et al., 2012), 9° (deMenocal et al., 2000)
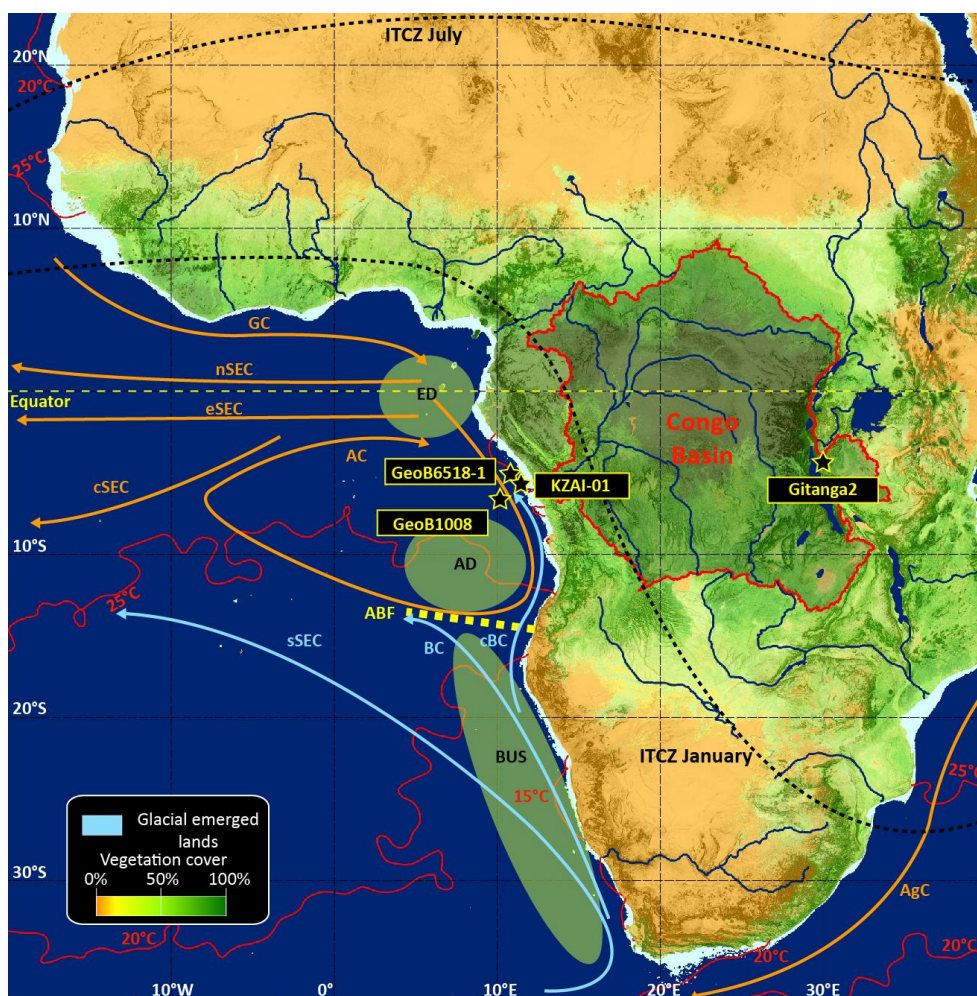914 Established palynozones subdivisions are also displayed (aX, bX; cf. Figures 4 and 5).
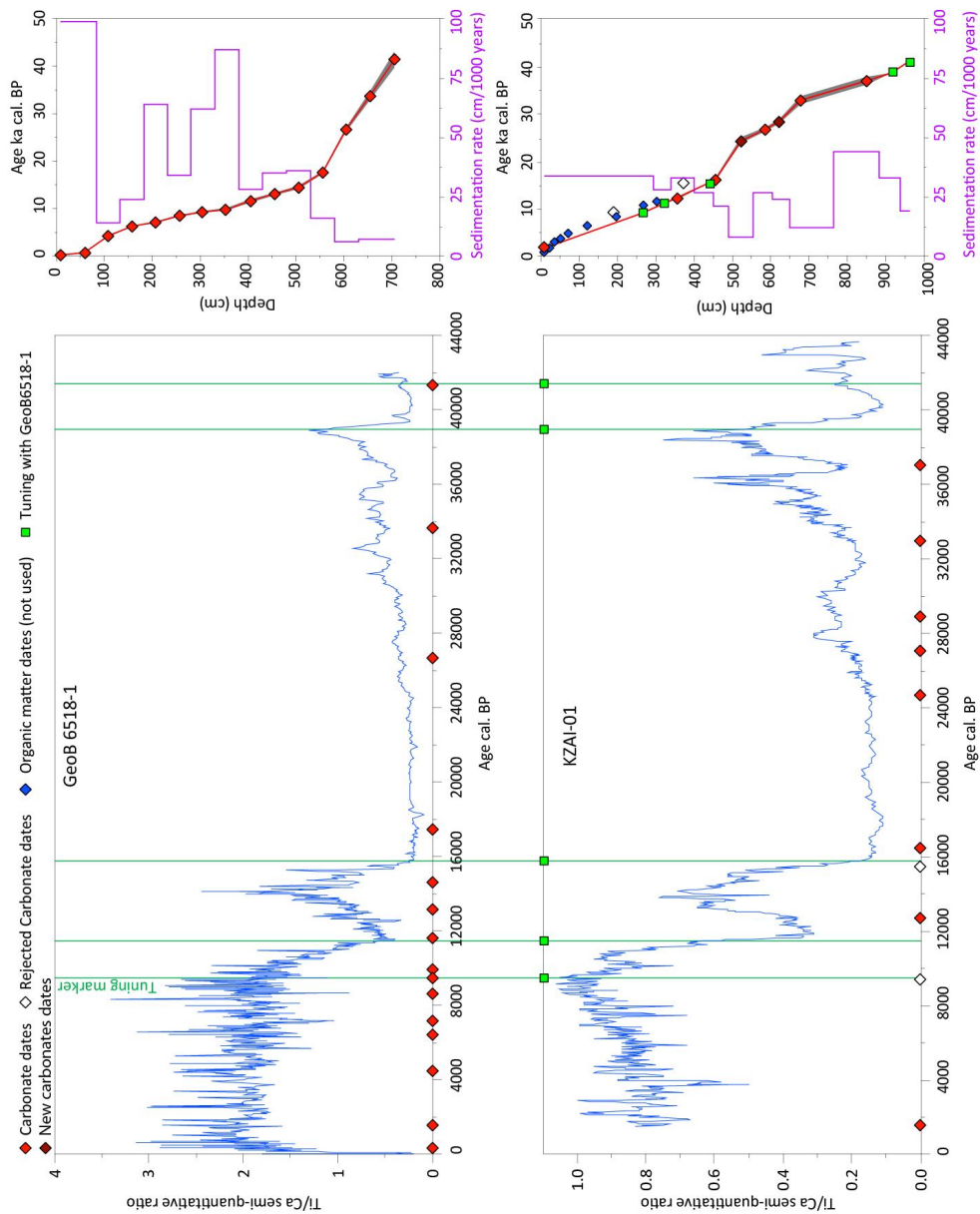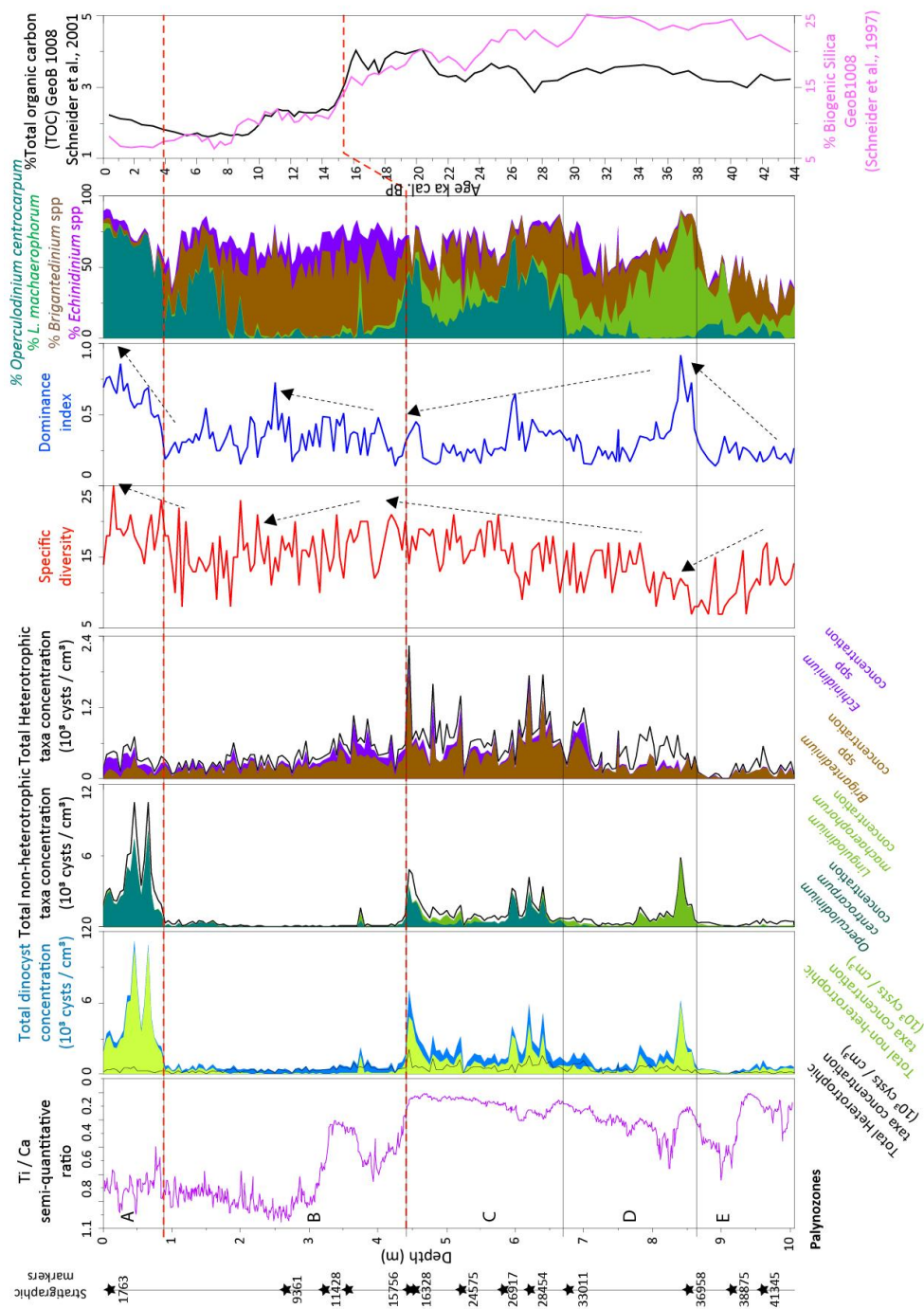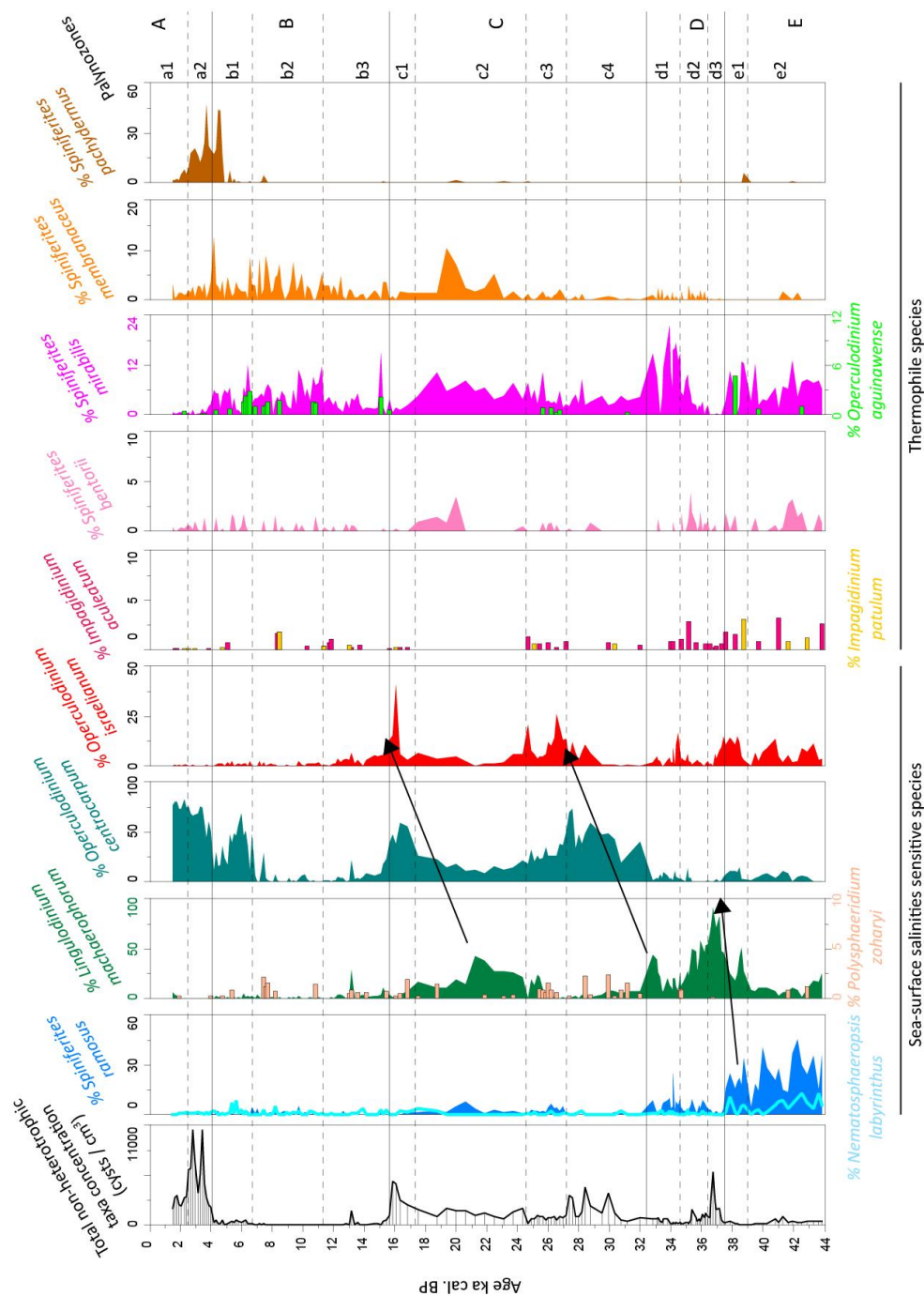915
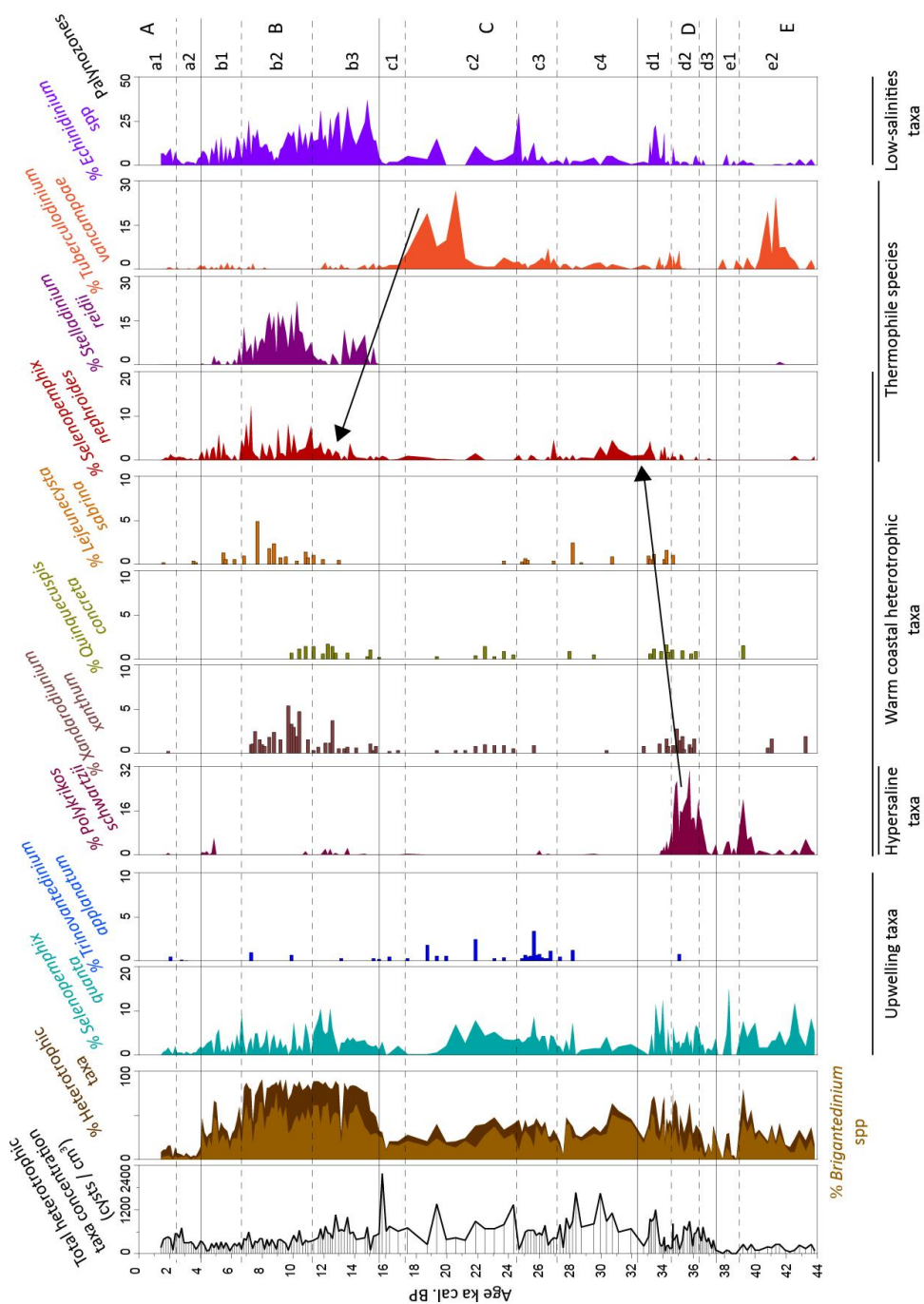916
917

918
919

920
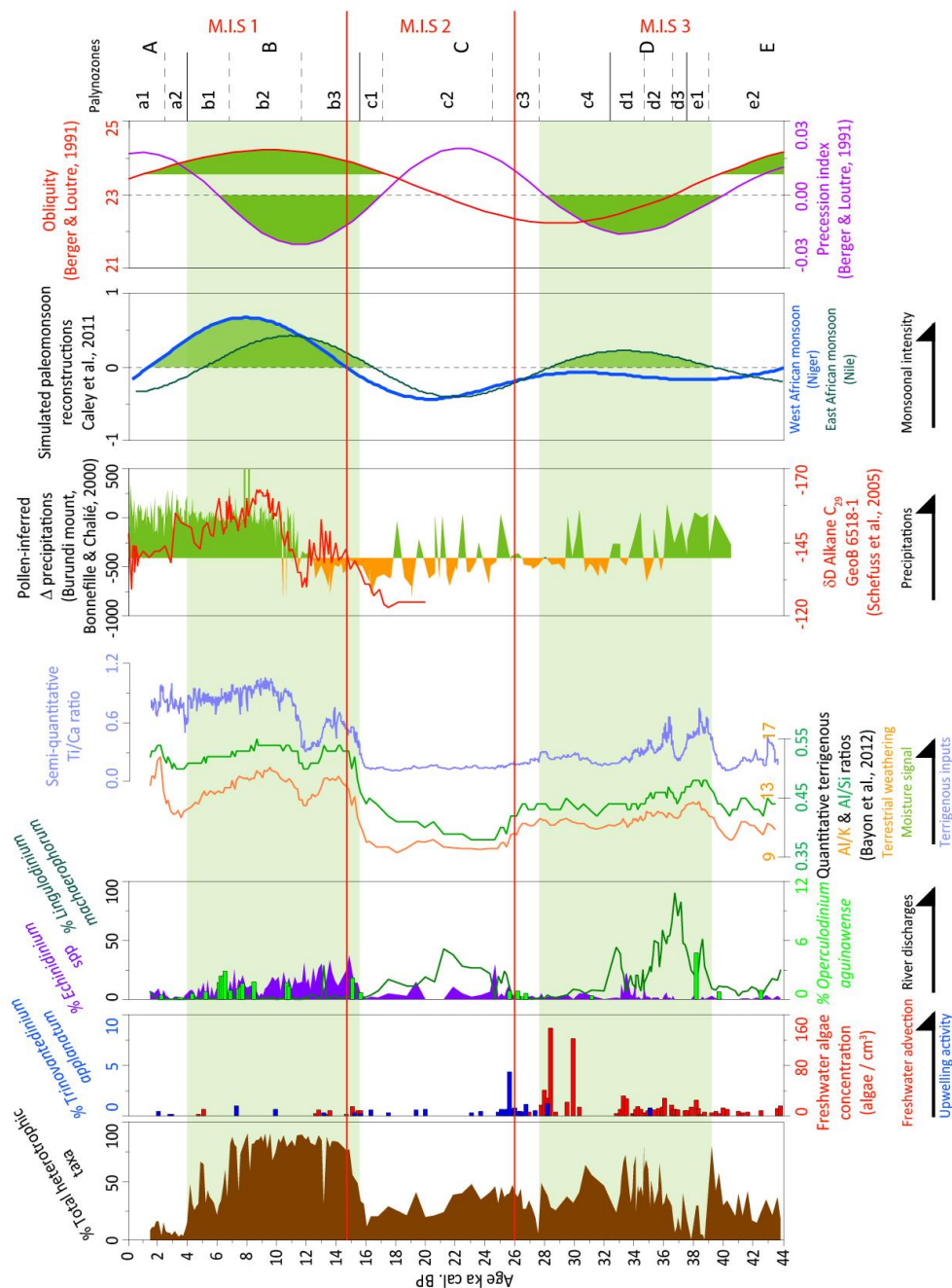921   Figure 1
922

923

924
925
926
927   Figure 2

928
929   Figure 3

930
931   Figure 4

932
933   Figure 5
934
935

936
937

938
939   Figure 6
940
941

942
943   Figure 7
944

Depth	Material	Laboratory number	Calendar age (BP)	Calibrated ^{14}C (cal. BP)	Data	Comments
10	Mixed marine carbonate	UtC-9311	2172 +/- 39	1763	Bayon et al., 2012	
13	*Bulk organic matter*	*Poz-40293*	*1610 +/- 30*	*1170*	*Bayon et al., 2012*	Not used
18	*Bulk organic matter*	*Poz-40295*	*2310 +/- 30*	*1921*	*Bayon et al., 2012*	Not used
26	*Bulk organic matter*	*Poz-40296*	*2545 +/- 30*	*2216*	*Bayon et al., 2012*	Not used
37	*Bulk organic matter*	*Poz-40297*	*3210 +/- 30*	*3024*	*Bayon et al., 2012*	Not used
51	*Bulk organic matter*	*Poz-40298*	*3770 +/- 30*	*3713*	*Bayon et al., 2012*	Not used
70	*Bulk organic matter*	*Poz-40299*	*4435 +/- 35*	*4636*	*Bayon et al., 2012*	Not used
122	*Bulk organic matter*	*Poz-40300*	*5970 +/- 40*	*6380*	*Bayon et al., 2012*	Not used
190	*Mixed marine carbonate*	*UtC-9312*	*8710 +/- 60*	*9369*	*Bayon et al., 2012*	Rejected
196	*Bulk organic matter*	*Poz-40301*	*8080 +/- 40*	*8527*	*Bayon et al., 2012*	Not used
265	Tuning with GeoB6518 core			9361	This paper	
269	*Bulk organic matter*	*Poz-40302*	*9790 +/- 50*	*10727*	*Bayon et al., 2012*	Not used
305	*Bulk organic matter*	*Poz-40389*	*10400 +/-*	*11503*	*Bayon et al., 2012*	Not used
322	Tuning with GeoB6518 core			11428	Bayon et al., 2012	
356	Planktonic foraminifera	Poz-20108	10930 +/-50	12444	Bayon et al., 2012	
372	*Bivalv*	*Poz-73781*	*13450 +/-70*	*15598*	*This paper*	Rejected
444	Tuning with GeoB6518 core			15756	Bayon et al., 2012	
456	Planktonic foraminifera	Poz-20109	13950 +/-70	16328	Bayon et al., 2012	
522	*Bolivina spatulatha*	Poz-73782	20800 +/-	24575	This paper	
585	Planktonic foraminifera	Poz-20110	23020 +/-	26917	Bayon et al., 2012	
622	Bivalv	Poz-73783	24870+/-	28454	This	
678	Mixed marine carbonate	UtC-9314	28240+/-280	31812	Bayon et al., 2012	
851	Mixed marine carbonate	UtC-9315	31800+/-400	35350	Bayon et al., 2012	

915	Tuning with GeoB6518 core			38875	This paper	
962	Tuning with GeoB6518 core			41345	This paper	

945   Table 1